

## A MINIMAL MODEL FOR PREDICTING VENTILATION RATES OF SUBTERRANEAN CAVES

Karina Khazmutdinova<sup>1,C</sup>, Doron Nof<sup>1,2</sup>, Darrel M. Tremaine<sup>3</sup>, Ming Ye<sup>1,2</sup>, M.N.J. Moore<sup>1,4</sup>

---

### ABSTRACT

The ventilation of carbon dioxide within subterranean caves regulates the growth of speleothems: mineral deposits found in caves that provide important clues about past climate. While previous studies have used internal temperature measurements to predict ventilation rates, such data would not be available for the task of climate reconstruction. Here, we develop a parsimonious model to predict ventilation rates from knowledge of outside temperatures and the cave's physical dimensions only. In the model, ventilation arises from buoyancy-driven flows created in passageways that connect to the outside. A few key simplifications lead to a system amenable to perturbation analysis, resulting in explicit expressions for ventilation rates. We compare these predictions to time-resolved, *in-situ* measurements of transported cave gases (carbon dioxide and radon). The theory accurately accounts for the timing and magnitude of seasonal and synoptic variations of these gases, and is, therefore, diagnostic of potential seasonal biases in speleothem growth. With proper *in situ* geochemical calibrations, this model may be used to establish a first-order estimate of atmospheric paleotemperatures.

---

### Introduction

Subterranean caves contain calcium-carbonate ( $\text{CaCO}_3$ ) mineral deposits, known as speleothems, which record important clues about past climate. Much like tree-rings and ice cores, these deposits can be used to infer past conditions and identify major climatic shifts (Wang et al., 2008). Speleothem records, however, can be difficult to interpret due to a number of competing factors that influence chemical and isotopic composition, mineral fabric, and timing of deposition (Frisia et al., 2000; Fairchild et al., 2006; Lachniet, 2009; Fairchild and Baker, 2012; Wong and Breecker, 2015). Early cave researchers realized the potential importance of internal cave conditions (Hendy, 1971), but only within the past twenty years has *in situ* monitoring technology become sufficiently advanced to record microclimate data with which to calibrate speleothem records (Perrier et al., 2005; Spötl et al., 2005; Baldini et al., 2006; Banner et al., 2007; Kowalczyk and Froelich, 2010; Tremaine et al., 2016). Recent laboratory studies and modeling efforts have further suggested that strong ventilation impacts processes such as evaporation and gas exchange across the thin water-film atop stalagmites, and therefore, the rate, timing, and isotopic composition of speleothems (Wackerbarth et al., 2010; Deininger et al., 2012; Dreybrodt et al., 2016; Hansen et al., 2017, 2019). These studies highlighted the fact that to fully understand a speleothem paleoclimate record, it is necessary to have a holistic understanding of the site-specific parameters that control stalagmite growth. These include, but are not limited to, rainfall amount, hydrologic saturation, vegetation and soil productivity, dripwater residence time and water-rock interaction, drip rates, and ventilation (Fairchild and Baker, 2012).

Speleothems are the end product of a series of chemical reactions: (1) rainwater combines with soil-zone carbon dioxide to form carbonic acid:  $\text{H}_2\text{O} + \text{CO}_{2(g)} \rightarrow \text{H}_2\text{CO}_3$ , (2) carbonic acid percolates downward and slowly dissolves carbonate bedrock, creating a high  $p\text{CO}_2$  solution of calcium and bicarbonate:  $\text{H}_2\text{CO}_3 + \text{CaCO}_3 \rightarrow \text{Ca}^{2+}_{(aq)} + 2\text{HCO}^{-}_{3(aq)}$ , and (3) the drip reaches a cave void, where the gradient between low- $p\text{CO}_2$  cave air and high- $p\text{CO}_2$  dripwater causes the drip to degas  $\text{CO}_2$ , driving the pH of the solution up and causing re-precipitation of calcium carbonate:  $\text{Ca}^{2+}_{(aq)} + 2\text{HCO}^{-}_{3(aq)} \rightarrow \text{CO}_{2(g)} + \text{H}_2\text{O} + \text{CaCO}_3$ . Cave ventilation modulates cave air  $\text{CO}_2$  concentration and thus the gradient between air and drip, driving both the timing and the vigor of speleothem growth. Without ventilation, cave air  $\text{CO}_2$  would come to chemical equilibrium with dripwater  $\text{CO}_2$ , and speleothem formation would cease.

In addition to controlling the rate and timing of deposition, ventilation has been shown in several long-term cave monitoring studies to have significant impacts on the isotopic composition of dripwater and subsequent speleothem calcite (Spötl et al., 2005; Frisia et al., 2011; Lambert and Aharon, 2011; Tremaine et al., 2011; Feng et al., 2012). Results from other field, theoretical, and laboratory studies support the hypothesis that under strong ventilation regimes where  $\text{CO}_2$  is quickly removed from dripwater, rapid precipitation may induce kinetic isotope fractionation, causing a shift in oxygen and carbon isotopes within the speleothem and making paleoclimatic interpretation of the record much more difficult (Scholz et al., 2009; Polag et al., 2010; Watkins et al., 2013, 2014; Stoll et al., 2015). A study by Daëron et al. (2019)

---

<sup>1</sup> Geophysical Fluid Dynamics Institute, Florida State University, USA.

<sup>2</sup> Department of Earth, Ocean, and Atmospheric Science, Florida State University, USA.

<sup>3</sup> Environmental Science Institute, Jackson School of Geosciences, University of Texas at Austin, USA

<sup>4</sup> Department of Mathematics, Florida State University, USA.

<sup>C</sup> Corresponding Author: kk11m@my.fsu.edu

recently demonstrated that even at extremely slow precipitation rates, such as those of subaqueous mammillary calcite in Devils Hole Cave (Nevada, USA), inorganic calcite suffers from kinetic fractionation effects in natural earth-surface systems. Indeed, these effects make the study of ventilation imperative for interpretation of speleothem oxygen and carbon isotopes.

Because ventilation controls the rate of calcite precipitation, it not only influences when a speleothem forms (which seasons), but also where the speleothem forms (i.e., on or within the cave ceiling (stalactite) or on the cave floor (stalagmite)). Wherever dripwater encounters low-CO<sub>2</sub> cave air, there is a potential for calcite precipitation up-stream of the stalagmite. This phenomenon is known as Prior-Calcite-Precipitation, or PCP (Fairchild et al., 2000). When PCP occurs, dripwater cation-to-calcium (X/Ca) ratios change as Ca is preferentially removed from solution, and minor elements such as Sr and Mg become more concentrated (Fairchild and Baker, 2012). PCP is often associated with climate-driven water balance above the cave, where more/less rainfall and thus hydrologic saturation above the cave results in higher/lower drip rates, lower/higher PCP, and lower/higher speleothem X/Ca ratios (Karmann et al., 2007; McDonald et al., 2007; Tremaine and Froelich, 2013; Tadros et al., 2016). Additionally, strong ventilation and low cave-air CO<sub>2</sub> promotes PCP and can exert control on variations in speleothem X/Ca ratios (Sherwin and Baldini, 2011; Wong et al., 2011). It is this seasonal variation in PCP, along with enhanced kinetic isotope effects during stronger ventilation, that will allow our ventilation model to be run in reverse to estimate the seasonality of atmospheric temperature differences.

Given that the process of cave ventilation can have significant impacts on the isotopic and trace element composition of modern calcite, we must endeavor to understand the ventilation of each cave that contains speleothems of paleoclimatic importance. This is especially true in light of recent work that recognized how cave ventilation varies seasonally with well-defined global patterns (James et al., 2015). While past studies have quantified cave ventilation in terms of internal temperature measurements (De Freitas and Littlejohn, 1987; Christoforou et al., 1996; Gregorič et al., 2014), such data would not be available for the task of climate reconstruction. Instead, predictive models must be developed.

Here, we construct a theoretical framework to predict ventilation rates from a minimal set of external information. Building on previous work (Wigley and Brown, 1971; De Freitas and Littlejohn, 1987; Christoforou et al., 1996; Kowalczk and Froelich, 2010), we model ventilation as arising from buoyancy-driven flows created by the internal-external temperature difference. Unlike previous studies, our model does not rely on any internal measurements. It only requires basic physical parameters of the cave itself and outside temperature data. To close the model, we require the flow to be critical via the composite Froude number, a condition borrowed from the field of oceanography (Armi, 1986; Dalziel, 1991; Pratt, 2008). Analysis of the relevant scales, along with a few key simplifications, produces a system that can be solved through perturbation methods, ultimately giving explicit formulas for how ventilation depends on the system's physical parameters.

To test our ventilation model, we use two tracers common to all limestone caves; carbon dioxide (CO<sub>2</sub>) and radon-222 (<sup>222</sup>Rn). As previously discussed, cave air CO<sub>2</sub> is derived from microbial decay and plant-root respiration in the soil zone, as well as dissolved limestone bedrock. Cave air CO<sub>2</sub> concentrations are modulated by a combination of input from both dripwaters and gaseous transport through cracks and fissures above the cave, import of atmospheric CO<sub>2</sub> via ventilation, and removal via condensation corrosion (Sánchez-Moral et al., 1999; Gabrovšek and Dreybrodt, 2000; Matthey et al., 2016). <sup>222</sup>Rn is a daughter isotope in a radioactive decay chain that begins with <sup>238</sup>U and ends with <sup>206</sup>Pb. Limestone contains an average 1.3 ppm <sup>238</sup>U to 2.5 ppm <sup>238</sup>U, and therefore, acts as a continuous source of radon production and advection into cave chambers through dripwaters, surfaces, and cracks (Fernández et al., 1986; Haki et al., 1997). <sup>222</sup>Rn is an ideal tracer for cave ventilation because atmospheric concentrations of radon are negligible and it is an inert gas with a 3.82-day half-life, which is sufficiently long when compared with most cave-air exchange rates (Fernández et al., 1986; Perrier et al., 2005; Richon et al., 2005; Kowalczk and Froelich, 2010). We report a set of time-resolved measurements of cave air gas concentrations from a cave located in Florida Caverns State Park. The theory accounts for qualitative trends in the measurements throughout the year, and, over certain periods, even shows quantitative agreement with weekly-scale fluctuations. This comparison also allows the production rates of CO<sub>2</sub> and <sup>222</sup>Rn to be estimated, which could complement other, more invasive, estimation techniques (Faimon et al., 2006; Kowalczk and Froelich, 2010).

## Study Site and Micrometeorological Station

Dragon's Tooth Cave (DTC) is a pristine, karst-hosted dry cave located in Florida Caverns State Park, Marianna, northwest Florida (Fig. 1a-b). The cave formed within a carbonate bluff along the nearby Chipola River, and has two primary passages that trend northwest to southeast in alignment with regional bedrock fractures. The two large passages are intersected by a third east-west trending corridor that dips at approximately 45 degrees from west to east, serving as an entrance to both sections. The northern section was first surveyed and mapped in 1978. The floor of the northern section lies at 18 meters above sea level (ASL) and is composed of mud-clay, which is typical of caves in Marianna that are subjected to seasonal groundwater inundation when Chipola River levels exceed 3–4 meters above the

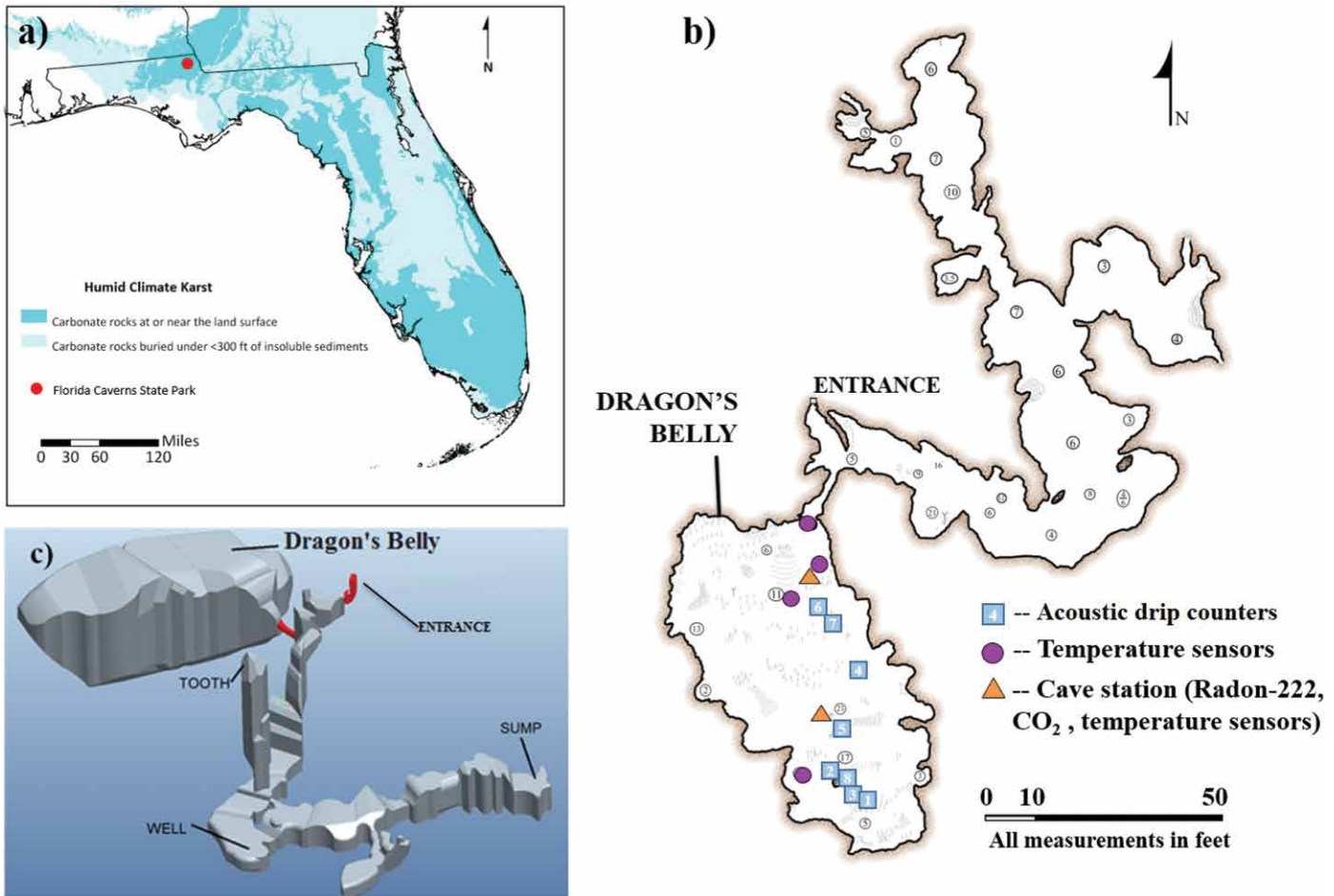


Figure 1. Study site: (a) Karst areas in Florida, USA (data is obtained from <https://pubs.usgs.gov/of/2014/1156/downloads/>). (b) Dragon's Tooth is a system of caves which includes the main study site, the Dragon's Belly. Also shown are the locations of our sensors within the Dragon's Belly (colored symbols) and elevations (circled numbers). (c) A 3D rendering of the Dragon's Tooth Cave system shows the approximately rectangular geometry of the Dragon's Belly and the narrow passageway that connects to the entrance of the cave system (highlighted in red).

riverbed. Passages within DTC are 2–3 meters tall, thus floodwaters tend to fill the passages and remove any stalactites or soda straws that may have formed, minimizing the potential of flowstone decoration. In 1984, cavers observed airflow through a pile of breakdown near the entrance and dug a narrow tunnel making a connection to the southern section of the cave, finding a previously unexplored room that was highly decorated with beautiful speleothem formations. This room later came to be known as the Dragon's Belly (DB). The floor of the DB lies at 21 meters ASL; groundwater slowly fills the DB from below only during Chipola flooding events that exceed 5 meters above riverbed. Topography above the cave suggests that the DB is the remains of a large diameter NW-to-SE conduit that has collapsed at both ends of the room. In 2012, our group mapped the DTC using Leica ScanStationP20 to obtain highly accurate measurements of its dimensions. The main chamber of the DB is nearly rectangular, 41 m long, 12 m wide, and 6 m high with 45° slopes at each end of the room that pinch off at the ceiling, and it connects to the entrance of the cave system via a single, narrow passageway (0.6 m high, 0.3 m wide and 3 m long). These geometrically simple features make the DB an ideal site for testing basic ventilation models. Once a firm theoretical foundation is established, future studies could examine more complicated cave systems (e.g., complex geometries and/or multiple openings).

Beginning in November 2011, we established a micrometeorological monitoring program inside the DB to continuously collect spatial and temporal variations of  $^{222}\text{Rn}$ ,  $\text{CO}_2$ , temperature, and drip rates.  $^{222}\text{Rn}$  and  $\text{CO}_2$  levels were measured via two cave stations deployed 15-meters apart (Fig. 1b). These stations were equipped with Durrige RAD7 detectors to measure radon, LiCor-820 gas analyzers to measure  $\text{CO}_2$ , as well as Vaisala HMP45C temperature and relative humidity sensors. Four additional Onset HOBO Pro v2 External Temperature Data Loggers were also deployed throughout the DB. In May 2012, eight acoustic drip counters mounted on tripods were deployed under stalactites in the DB to measure drip rate (Fig. 1b). All data were recorded hourly, with the exception of occasional outages due to flooding events or power failures. Meanwhile, we obtained external temperature data from daily measurements taken at Marianna Municipal Airport, located 8 km from the study site.

## The Ventilation Model

We model the ventilation in DB's room as a well-mixed compartment with a single opening that exchanges heat with the surrounding surfaces and the outside environment. Because the internal cave temperature  $T_c$  is typically different from the external temperature  $T_e$ , a buoyancy-driven flow is created in the connecting passageway (Hunt and Linden, 1999; Pratt, 2008). During the summer, warm outside air flows into the DB through the top half of the opening, is cooled by contact with the cave walls, and exits through the lower half of the same opening. The airflow direction reverses during the winter (see Figs. 2a–b for a schematic). Faimon et al. (2012) showed that temperature accounted for more than 99 % of variations in cave air density. Therefore, we neglect secondary effects such as humidity and ambient pressure.

As long as vertical mixing and viscous effects are weak (i.e., large Peclet and Reynolds numbers), the flow in the opening is essentially that of two layers: a top layer of depth  $H_1$  and speed  $U_1$ , and a bottom layer with values  $H_2$  and  $U_2$ . In accordance with the Boussinesq approximation, we only take density variations into account insofar as they affect buoyancy (Boussinesq, 1897). Enforcing the Boussinesq approximation and conservation of volume inside the cave results in a symmetric exchange flow (i.e., both the depths and speeds are the same in the two layers)  $H_1 = H_2 = H$  and  $U_1 = U_2 = U$ . Clearly,  $H$  must be the half-height of the passageway ( $H = 0.3$  m), but  $U$  must be determined through other considerations, starting with a balance of the cave's total thermal energy.

### Thermal energy balance and closure condition

Under the assumptions of (1) well-mixed air inside the DB room, (2) the Boussinesq approximation, and (3) a symmetric two-layer exchange flow in the cave opening, the rate of change of the cave's thermal energy takes the form (Christoforou et al., 1996):

$$\rho_o c_v V \dot{T}_c = \rho_o c_p A U (T_e - T_c) + \int_s q dS \quad (1)$$

The main unknowns in this ordinary differential equation (ODE) are the cave's internal temperature,  $T_c$ , and the exchange speed,  $U$ . Meanwhile, the outside temperatures,  $T_e$ , will be taken from the measurements at Marianna Airport. The parameters are the mean air density  $\rho_o = 1.205$  kg/m<sup>3</sup>, the specific heat of air at constant pressure  $c_p = 1005$  J/(kgK) and at constant volume  $c_v = 717$  J/(kgK), the total volume of the cave chamber  $V = 2952$  m<sup>3</sup>, and the half-area of the cave passageway  $A = 0.09$  m<sup>2</sup>.

The first term on the right of Equation (1) represents thermal exchange with the outside via the two-layer flow, while the second represents exchange with the cave walls through surface integration of the local heat-transfer-per-unit-area  $q$  [J/(m<sup>2</sup>s)]. Temperature differences between these surfaces and the enclosed air give rise to convective flows that can promote heat transfer greatly. The Nusselt number, Nu (the ratio of convective to conductive heat transfer), quantifies this increase and can be estimated through knowledge of the Rayleigh number, . Here,  $T_w$  is the wall temperature and  $l$  is a length scale of the surface under consideration, while  $g = 9.8$  m/s<sup>2</sup> is the gravitational acceleration,  $\nu = 15.1 \times 10^{-6}$  m<sup>2</sup>/s and  $\alpha = 2.12 \times 10^{-5}$  m<sup>2</sup>/s are the viscosity and thermal diffusivity of air, and  $T_o = 291.9$  K is the mean annual temperature in Marianna, Florida. To estimate the Nusselt number, we use the well-established scaling law (Holman, 2002; Bergman and Incropera, 2011)

$$\text{Nu} = \chi \text{Ra}^{1/3}, \quad (2)$$

where  $\chi$  is a constant that depends on the orientation of the surface and the direction of the thermal gradient. The side-walls produce convection regardless of the sign of the temperature gradient, whereas the floor and ceiling only produce convection in the presence of an unstable temperature gradient (see Appendix A for further details). The above law holds for  $\text{Ra} > 10^7$ , and inside the DB's we typically have  $\text{Ra} \sim 10^{10}$ .

The local heat transfer on a particular surface is given by  $q = \rho_o c_p \alpha \text{Nu}_u (T_w - T_c) / l$  (Holman, 2002), and insertion of the Nu-Ra relationship gives

$$\int_s q dS = \rho_o c_p \left( \frac{g \alpha^2}{\nu T_o} \right)^{1/3} \int_s \chi (T_w - T_c)^{4/3} dS \quad (3)$$

Here, we have adopted the convention  $X^p = |X|^p \text{sgn } X$  for any variable  $X$  in order to shorten expressions. We will take the wall temperature,  $T_w$ , to be a different constant on each surface (i.e., the ceiling, the floor, and the four sidewalls) so that the integral in Equation (3) reduces to a summation over these six faces. We note that the length scale  $l$  has dropped out of Equation (3) as a consequence of the  $\text{Nu} \sim \text{Ra}^{1/3}$  law. Though easily overlooked, this cancellation simplifies the analysis considerably and avoids certain ambiguities in the definition of  $l$  (see Appendix A). This is one factor that will ultimately allow us to obtain closed-form expressions for the ventilation rate.

Both  $T_c$  and  $U$  are still unknown at this stage, and so a second relationship is required to close the model. Because the DB's is a single-opening room, we can leverage fundamental results from the study of two-layer exchange flows

(Armi, 1986; Dalziel, 1991; Pratt, 2008). Such flows have been found to spontaneously organize into a critical state, characterized in this context by a composite Froude number equal to one. Imposing this condition gives the speed of the exchange flow as

$$U = \sqrt{\frac{1}{2} \frac{HglT_e 2 T_c}{T_0}} \tag{4}$$

We note that other closure conditions could be used for caves with multiple openings, which we will explore in a future manuscript (Christoforou et al., 1996; Flynn and Caulfield, 2006).

**Estimating internal-surface temperatures**

Our main goal is to solve Equations (1) – (4) for the cave temperature,  $T_c$ , and the exchange speed,  $U$ , but first it is necessary to estimate the cave-wall temperatures,  $T_w$ , for insertion into Equation (3). Here, we will use temperature measurements from inside the cave to guide and validate certain approximations made in our model. Once constructed, though, the model will not rely on these internal measurements, and the same framework could be applied to other caves without any recalibration.

We begin with a formula often used in the design of wine cellars to estimate the underground temperature at a depth  $z$  (Pinchover and Rubinstein, 2005; Tinti et al., 2014),

$$T(z,t) = T_0 + \Delta T_e^{-z/z_0} \cos(\omega(t - t_0) - z/z_0) \tag{5}$$

Here,  $\omega = 1.99 \times 10^{-7}$  rad/s is the annual frequency,  $\Delta T = 9.3$  K is the amplitude of the seasonal temperature variation (illustrated by the dashed curve in Figure 2d),  $\alpha_{lim} = (5.6 \pm 1.6) \times 1027$  m<sup>2</sup>/s is the thermal diffusivity of the limestone medium,  $z_0 = \sqrt{2\alpha_{lim}/\omega} = 2.4 \pm 1.3$  m is the attenuation depth, and  $t_0$  simply sets an initial time. This formula neglects higher modes, for example diurnal and synoptic variations, since they attenuate much more rapidly with depth. The attenuation depth,  $z_0$ , depends on the physical properties of the local geology, thus, by using appropriate values for thermal diffusivity, temperatures of surfaces within caves formed in bedrock other than limestone can be calculated.

Equation (5) is an exact solution to a diffusion problem in a homogeneous domain with a periodically driven upper surface. Although the presence of the cave violates the homogeneity assumption, the much lower density of the enclosed air implies that a very large change in air temperature would be required to modify the limestone temperature

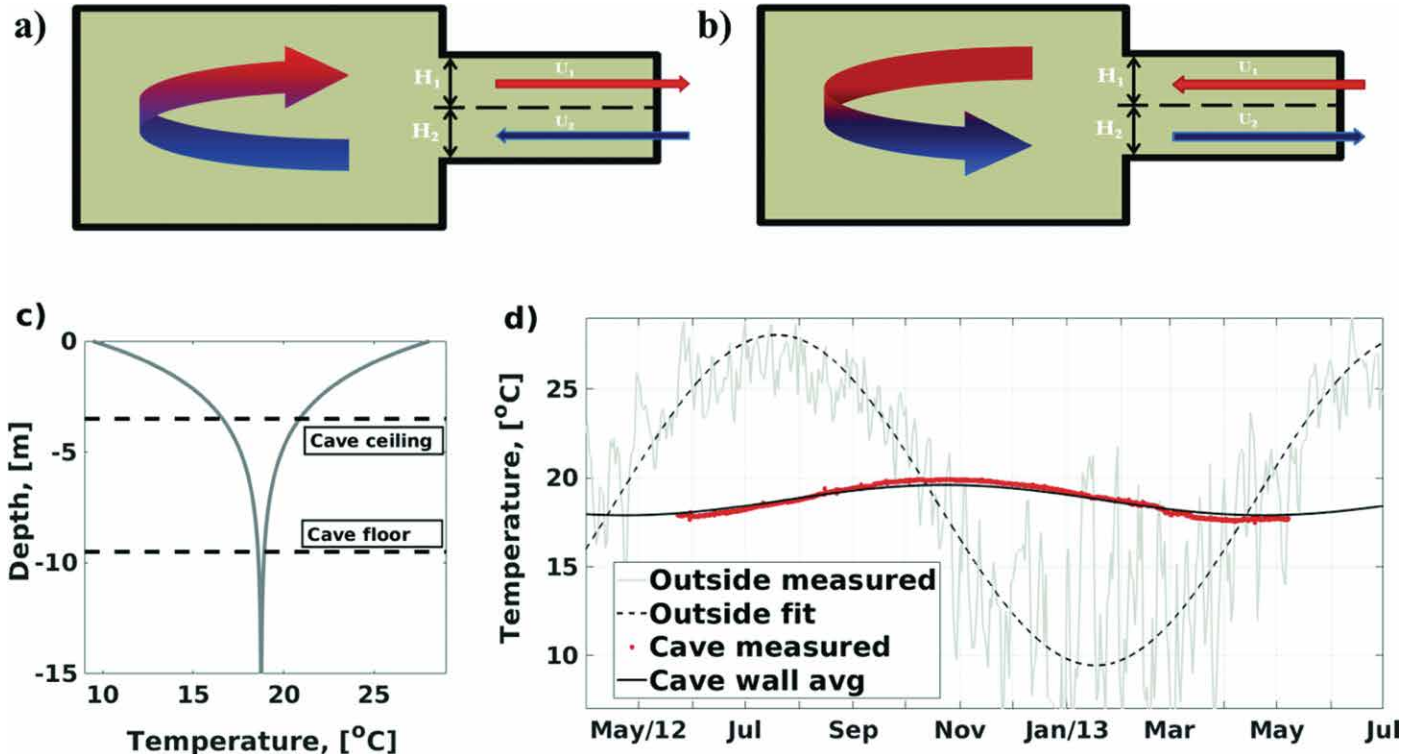


Figure 2. The ventilation model: (a) – (b) The temperature difference between the cave and the outside creates an exchange flow, regardless of whether the cave is (a) warmer or (b) cooler than the outside. (c) The temperature range at various depths as predicted by the wine-cellar formula, Equation (5), with the ceiling and floor of the Dragon’s Belly indicated. (d) The cave-wall temperatures can be estimated by inserting the outside temperatures (measurements in faint gray and seasonal fit in dashed black) into Equation (5). The solid black line shows the predicted average wall temperature, which agrees well with internal measurements (red).

appreciably. We therefore apply the formula to estimate the temperature of each cave surface. For the sidewalls, we estimate an average temperature by integrating the formula over the height of the wall with a 3-point trapezoid rule. Figure 2c shows the temperature range predicted by the wine-cellar formula as it varies with depth. Note that at approximately 12 m depth, the temperature of the ground becomes equal to the annual mean of the outside temperature, and there are no seasonal variations below 12 m. That 12 m depth depends on the physical properties of the local geology and varies depending on where the cave is formed. Notably, the temperature of the DB's ceiling varies over a much wider range than does the floor (by a factor of 12).

We next compare these predictions with temperature measurements taken inside the cave. Internal convective flows tend to homogenize the cave-air temperature, and so regardless of where the sensors are placed, the measurements are influenced by all of the surrounding surfaces. We therefore define an average wall temperature,  $T_{wa}$ , which incorporates the temperatures of the ceiling, floor, and sidewalls as weighted by surface area

$$T_{wa} = \frac{1}{S} \sum_{i=1}^6 S_i T_i \quad (6)$$

Here,  $T_i$  and  $S_i$  are the temperature and area of surface  $i$ , and  $S$  is the total surface area (1620 m<sup>2</sup>). Figure 2d shows the estimated  $T_{wa}$  (black) as it compares with measurements (red). The prediction captures the phase of the measurements very accurately and under-predicts the amplitude slightly. The under-predicted amplitude is of minor consequence when compared to the scale of the outside-temperature fluctuations, shown by the faint gray data in Figure 2d. Due to their larger magnitude, the outside-temperature fluctuations are primarily responsible for creating the inside/outside temperature difference that drives exchange.

Figure 2d provides one last insight. The predicted  $T_{wa}$  agrees well with internal measurements, even though it does not take ventilation into account. This suggests that the cave's thermal exchange is a wall-dominated process, a concept that is supported by the scaling analysis in Appendix C. It may seem paradoxical that, while ventilation is the main quantity we aim to predict, observations suggest it to be a secondary effect. The resolution is that, while ventilation is indeed secondary for thermal exchange, it is the primary transport mechanism for cave gases such as carbon dioxide and radon. By using simple internal-temperature estimates to predict ventilation rates, our model can accurately describe the transport of these gases.

### Predicting exchange rates

Having obtained reliable wall-temperature estimates, it is now possible to solve Equations (1) – (4) for the cave air temperature,  $T_c$ , and the speed of the exchange flow,  $U$ . Once  $U$  is known, the main quantity we seek is the ventilation rate

$$\lambda_v = AU/V, \quad (7)$$

which allows us to determine how cave gases are exchanged with the outside. We solve Equations (1) – (4) with two different approaches. The first is a numerical strategy that tracks the temperature of each individual cave surface and dynamically switches thermal convection on or off depending on the direction of the local temperature gradient. This model thus represents the complex physics of thermal convection with spatial and temporal resolution (see Appendix B for further details). The second approach is a course-grained model that assumes spatially uniform convection to arrive at a system amenable to perturbation analysis. This analysis ultimately gives an explicit expression for how the ventilation rate depends on cave and climatic parameters (see Appendix C for details). With these two approaches, we have both the physical fidelity offered by a computational model and the transparency offered by a purely analytical model. Comparison between the two will allow us to test the additional assumptions made in the perturbation model.

As described in Appendix C, analysis of the relevant physical scales identifies two dimensionless parameters,  $\pi_1$  and  $\pi_2$ . Briefly,  $\pi_1$  represents the timescale of wall-thermal exchange compared to the timescale of the outside temperature variation (i.e., a year), while  $\pi_2$  represents the relative strength of ventilation-induced versus wall-induced thermal exchange. In terms of these parameters, perturbation analysis gives the ventilation rate as

$$\lambda_v \sim \frac{A}{V} \sqrt{\frac{Hg}{2} \left| \frac{T_{wa} - T_e}{T_0} \right|^{1/2}} \left( 1 - 0.5 \left( \frac{\pi_2}{\chi_0} \right)^{3/4} \left| \frac{T_{wa} - T_e}{T_0} \right|^{1/8} \right), \quad \pi_2 \ll 1 \quad (8)$$

This formula shows that the ventilation rate depends primarily on the absolute difference between the cave-wall temperature,  $T_{wa}$ , and the outside temperature,  $T_e$ . The term involving  $\pi_2$  represents nonlinear damping of ventilation due to the internal air adjusting to the outside temperature. For the DB's room, this term only makes a 1 % contribution. However, caves with less idealized features may experience a larger contribution from this term, and future studies on such caves could allow us to examine it more closely.

Once  $\lambda_v$  is known (from either the numerical or perturbation model), we can determine how cave gases, namely carbon dioxide and <sup>222</sup>Rn, are exchanged with the outside environment. The transport of either quantity can be described by the ODE

$$\dot{C} = \frac{S}{V} \Phi - \lambda_V(C - C_e) - \lambda_r C \tag{9}$$

where  $C$  is the concentration of  $\text{CO}_2$  [ppmv] or activity of  $^{222}\text{Rn}$  [ $\text{Bq}/\text{m}^3$ ] inside the cave (Kowalczk and Froelich, 2010). The first term on the right represents the flux of  $\text{CO}_2$  or radon into the cave through internal surfaces. We assume the production term of either gas,  $\Phi$ , to be constant and will first estimate its value from measurements and then tune the production term to minimize errors. The second term on the right represents exchange with the outside via ventilation. Here,  $C_e$  is the external concentration, where  $C_e = 392$  ppmv for  $\text{CO}_2$  and  $C_e$  is negligible for  $^{222}\text{Rn}$ . The last term on the right represents decay of  $^{222}\text{Rn}$ , where  $\lambda_r = 2.1 \times 10^{-6} \text{ s}^{-1}$  (this term is zero for  $\text{CO}_2$ ).

### Results: Field Measurements and Theoretical Predictions

We now discuss the measurements taken at the DB's site, shown by the red curves in Figures 3a-c for  $\text{CO}_2$  and Figures 3d-f for  $^{222}\text{Rn}$ . Cave air gas concentrations in the DB were collected at 30-minute intervals over a 14-month period, with occasional interruptions due to flooding and/or power outages. Both the perturbation model and the numerical model were performed with a 24-hour resolution. Models and measured data are plotted together in Figure 3. The highest concentrations of cave gases occur during fall and spring, while the lowest concentrations occur during summer, followed by winter. This result is counter to those in caves under predominantly chimney-driven airflow regimes that promote strong winter-time ventilation (e.g., Obir Cave (Spötl et al., 2005), Inner Space Caverns (Banner et al., 2007), and Hollow Ridge Cave (Kowalczk and Froelich, 2010)).

During the winter, carbon-dioxide levels in the DB are near their minimum, while radon levels are intermediate. Qualitatively, these trends suggest ventilation to be lowest during fall and spring, when daily average inside-outside temperature differences are small, and highest during summer and winter, when the temperature differences are maximal. The observations support the idea of ventilation being caused primarily by buoyancy-driven flows.

Predictions of  $\text{CO}_2$  and  $^{222}\text{Rn}$  are shown by the dark curves in Figure 3. The gray curves represent the numerical model, with convection switched on/off for each surface individually, while the black curves show the perturbation solution given by Equation (8). The two predictions are nearly indistinguishable, providing validation for the additional assumptions made in the perturbation model. We estimate the source term,  $\Phi$ , by minimizing the difference between model simulations and measurements, giving  $\Phi = 3.1 \times 10^{-9} \text{ kg}/(\text{m}^2\text{s})$  for  $\text{CO}_2$  and  $\Phi = 25 \times 10^{-6} \text{ kBq}/(\text{m}^2\text{s})$  for  $^{222}\text{Rn}$ . We note that our estimated source terms for  $^{222}\text{Rn}$  and  $\text{CO}_2$  are comparable to those found in the literature (e.g., for  $^{222}\text{Rn}$ :  $\Phi = 9.9 \times 10^{-6} \text{ kBq}/(\text{m}^2\text{s})$  (Faimon et al., 2006) and  $\Phi = 13 \sim 61 \times 10^{-6} \text{ kBq}/(\text{m}^2\text{s})$  (Kowalczk and Froelich, 2010); for  $\text{CO}_2$ :  $\Phi = 1.989 \times 10^{-10} \text{ kg}/(\text{m}^2\text{s})$  (Baldini et al., 2006) and  $\Phi = 1.56 \times 10^{-9} \text{ kg}/(\text{m}^2\text{s})$  (Faimon et al., 2006)).

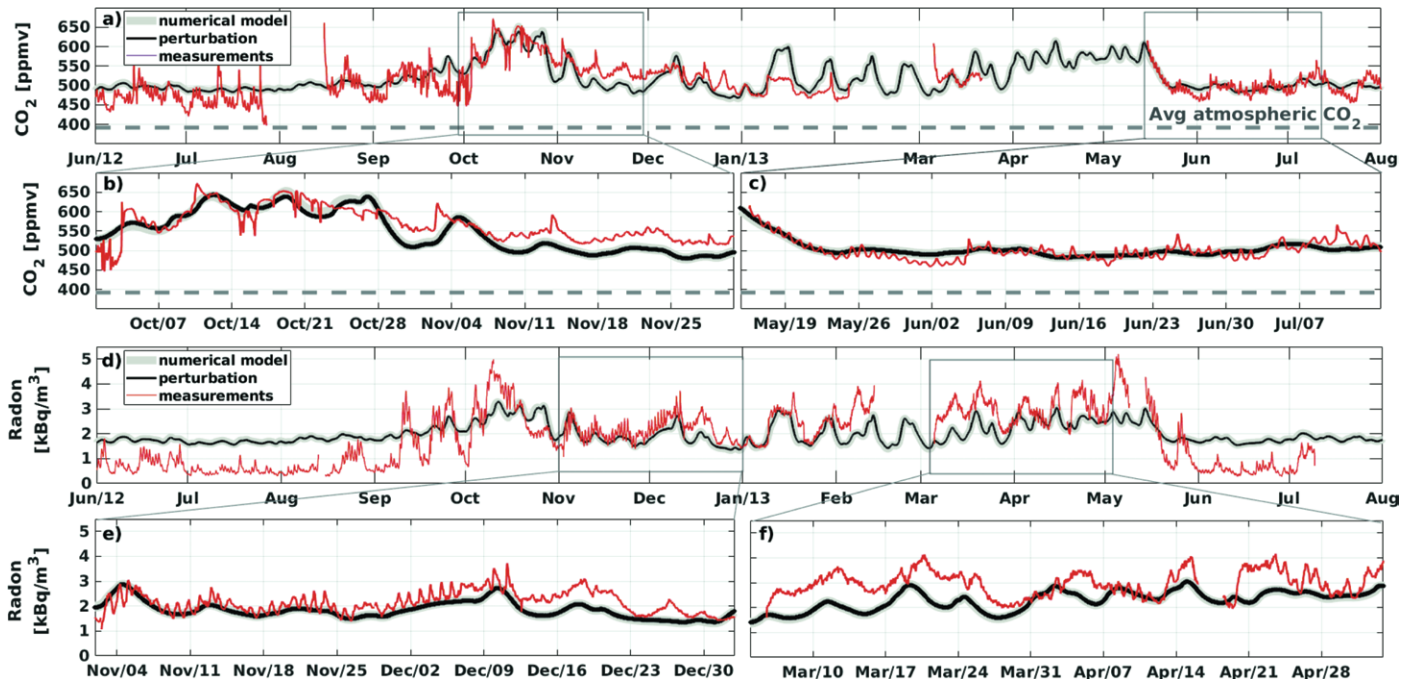


Figure 3. Variations of *in situ* gas concentrations. (a) The measured levels of  $\text{CO}_2$  (red) over the full 14-month period, along with predicted values from the numerical model (gray) and the perturbation solution (black), the two of which are nearly identical. (b) – (c) Zoom of selected date ranges offers a closer comparison. (d) – (f) Similar plots for  $^{222}\text{Rn}$ . Notice both gases show prominent variations on a near-weekly timescale, and the theory exhibits similar fluctuations.

With the source term as the only fitted parameter, both the CO<sub>2</sub> and radon predictions correspond well with measurements over the majority of the 14-month study. In particular, the model accounts for the higher levels of cave gases in the fall/spring and lower levels in the summer/winter. The only obvious discrepancy is in comparing radon levels in the summer, where the theory predicts a significantly higher level than was measured. Carbon dioxide shows good agreement during this same period, though, suggesting the discrepancy to be specific to radon.

While not a focus of this study, hydrologic conditions within the rock above the DB may have a significant influence on agreement between modeled and measured <sup>222</sup>Rn over seasonal time periods. Andrews and Wood (1972) demonstrated that radon emanation from limestone occurs from within a mineral surface layer only a few microns thick, and that under dry conditions, alpha-recoil causes radon gas to be ejected from the crystal lattice into inter-crystal cracks and imperfections, eventually to find its way out of the limestone through relatively slow diffusion in air at the rate of approximately 10<sup>-2</sup> cm<sup>2</sup>/s. Conversely, under wet conditions within the epikarst, alpha-recoil can cause radon particles to be ejected from the crystal lattice directly into pore water. As dripwater percolates downward, it has a scavenging effect, driving a significantly higher flux of radon during periods when the epikarst is wetter. An excellent example of this phenomenon was illustrated by Kowalczyk and Froelich (2010) at Hollow Ridge Cave, when a tropical storm delivered 83 mm of rainfall, wetting the epikarst and causing a nearby river to flood and plug up the lower entrances of the cave, temporarily ceasing ventilation. Directly following this rainfall, <sup>222</sup>Rn-emanation rates increased from normal 48–222 Bq m<sup>-2</sup> hr<sup>-1</sup> to approximately 1200 Bq m<sup>-2</sup> hr<sup>-1</sup>. Unpublished data from laboratory testing of limestone from both DTC and Hollow Ridge Cave confirms that wet transport can increase <sup>222</sup>Rn emanation by 1.6–2.4 times dry transport (William Burnett – FSU, personal communication to Khazmutdinova and Tremaine, 2015).

Figure 4 illustrates that prior to August 2012, most of the monitored drip rates were essentially zero. During August, a 120 mm rainfall and several successive ~40 mm rainfalls prompted increased pore water within the overburden. Approximately 1–2 weeks after each event, an increase in <sup>222</sup>Rn was observed, followed by a decay to background levels. In September 2012, all monitored sites rapidly increased in drip rate as the epikarst reached some saturation threshold. These conditions persisted until May 2013, when lower rainfall and increased evapotranspiration reduced pore water storage below the saturation threshold, causing measured radon to again fall below values predicted by our model.

In addition to the seasonal variation, the CO<sub>2</sub> and <sup>222</sup>Rn measurements show more rapid fluctuations on a few characteristic scales. Figures 3b-c and Figures 3e-f zoom on selected date ranges to highlight the rapid fluctuations. First, the measurements show very rapid, diurnal fluctuations, which resulted from the different day/night temperatures. In the model, we only input daily outside temperatures, and so these very fast fluctuations are not present. Presumably they could be captured with more temporal resolution (e.g., hourly readings). Interestingly, there is a second, intermediate

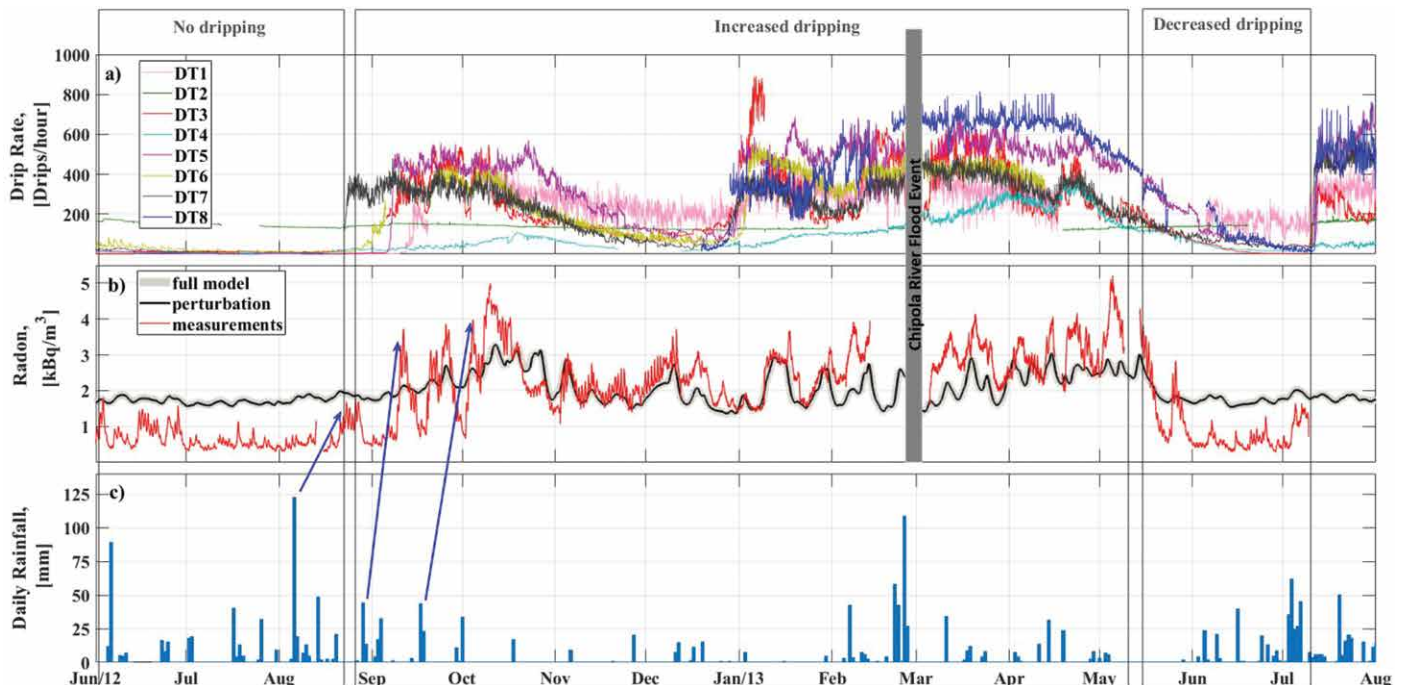


Figure 4. Time series of measured drip rate, <sup>222</sup>Rn concentration, and daily rainfall. (a) The measured drip rates at eight locations within the Dragon's Belly. (b) The measured levels of radon (red) over the full 14-month period, along with predicted values from the numerical model (grey) and the perturbation solution (black). (c) Daily rainfall above Dragon's Belly. Blue arrows indicate radon response to several successive rainfalls.

timescale (on the order of 5–9 days) that is also evident in the  $\text{CO}_2$  and  $^{222}\text{Rn}$  data. This nearly weekly cycle is likely influenced by synoptic-scale meteorology (Holton and Hakim, 2012) although human activity may play a role too (Daniel et al., 2012; Earl et al., 2016). Regardless, the model shows variations over exactly the same scale. This implies that the weekly cycle in cave-gas levels is ultimately tied to a weekly cycle in outside temperatures that drives an exchange flow as described by our theory. Over certain periods, for example those shown in Figure 3e, the theory even shows quantitative agreement with tracer measurements.

## Discussion: Implications for Paleotemperature Modeling

Here we develop the logical framework for combining this ventilation modeling approach with several important *in-situ* geochemical calibrations that parameterize variations in modern isotope and X/Ca ratios in calcite. This synthesis of modeling and empirical field data engenders a first-order estimation of monthly and annual atmospheric air temperature, as well as length of seasons.

Until recently, subsampling a speleothem for powders from individual growth bands was restricted to the technical limits of physically machining the mineral surface with a drill press or micromill to produce powders. Because the average speleothem precipitates at a rate of 100–500  $\mu\text{m}/\text{y}$ , it would be necessary to mill at approximately 8–41  $\mu\text{m}$  (monthly resolution) to investigate seasonal ventilation, well below the limits of moderately priced technology. Advances in Inductively Coupled Plasma Mass Spectrometry (ICP-MS) during the last ten years has vastly increased sample resolution, specifically in carbon and oxygen isotopes. Using ion-microprobe, investigators can determine precise oxygen isotope ratios in  $\text{CaCO}_3$  speleothems and foraminifera at sample sizes as small as 6–10  $\mu\text{m}$  (Kozdon et al., 2009; Orland et al., 2012). Chen et al. (2017) developed Laser Ablation (LA) ICP-MS techniques to measure carbon isotope ratios in magmatic and hydrothermal calcites, achieving results that agreed well with conventional Isotope Ratio (IR)-MS methods, but on spot sizes of only 33  $\mu\text{m}$ . Together, these advancements allow for measurements of speleothem calcite isotopes at the same resolution as trace-elemental composition (via LA-ICP-MS), opening the door to using carbon, oxygen, and X/Ca ratios as concomitant proxies for seasonal ventilation strength and timing.

It is now well established that monitoring individual drip site chemistry is a necessary first step toward interpreting the speleothem forming from that drip (Fairchild and Baker, 2012). In order to calibrate modern ventilation to speleothem calcite, it is necessary to monitor the drip for incoming isotopes, as well as the partial pressure of  $\text{CO}_2$  ( $p\text{CO}_2$ ), pH, and X/Ca ratios, while simultaneously forming calcite under that drip and analyzing it to observe seasonal patterns in isotopes and X/Ca ratios (Mickler et al., 2004; Spötl et al., 2005; Banner et al., 2007; Tremaine, 2010, 2015). The cave site must be chosen such that calcite precipitates (1) year-round, and, (2) rapidly enough to precipitate sufficient mass of calcite to exchange farming plates on a monthly basis. Cave air  $\text{CO}_2$  and  $^{222}\text{Rn}$  production rates ( $\Phi$ ; Equation (9)) should be measured or closely estimated. Finally, the cave site must ventilate seasonally with sufficient strength to induce measurable variations in oxygen and carbon isotopes and X/Ca ratios within farmed calcite (see Tremaine et al., 2011; Wong et al., 2011), and be monitored at bi-weekly intervals for cave air  $\text{CO}_2$ , relative-humidity, temperature, and  $^{222}\text{Rn}$ . With all of these conditions met in an ideal cave site, it would be straightforward to create a calibration between modern seasonal ventilation strength, seasonal atmospheric temperatures, and seasonal changes in coeval farmed calcite isotopes and X/Ca ratios. These relationships may then be parameterized and incorporated into the ventilation model as ventilation ( $\lambda_v$ ; Equation (8)) and  $\text{CO}_2$  (C; Equation (9)).

By tuning our model to the specific dimensions of the studied cave site, these quantitative relationships can be applied backwards in time. First, the speleothem would be analyzed for isotopes and trace elements over small sections at monthly resolution (33  $\mu\text{m}$  spot size for an axial extension of  $\sim 400 \mu\text{m}/\text{y}$ ). The model would be inverted and tuned to match the strength of ventilation, with the output being the difference in temperature between the cave and the atmosphere during ventilation season. By knowing the relationships between seasonal changes in modern ventilation strength and concomitant changes in calcite isotopes and X/Ca ratios, this approach would allow a first order estimation of the temperature difference between atmosphere and cave air temperature. By comparing monthly atmospheric temperature profiles, one could infer average annual temperature, and length of seasons. We acknowledge that this approach requires the assumption that no major changes in cave morphology have occurred during the life-span of the speleothem under analysis, which is never guaranteed, and therefore, this approach may give insight that is only semi-quantitative.

## CONCLUSIONS

In this study, we constructed a theoretical framework to predict cave ventilation rates from a minimal set of external information, namely knowledge of the outside temperature and the physical dimensions of the cave. The major advantage is that external temperatures are much more easily accessible than microclimate conditions inside the cave. Through scaling analysis and a few key modeling assumptions, we obtained explicit relationships for how ventilation depends on system parameters given by Equation (8). Comparison with time-resolved, *in-situ* measurements demonstrates that the theory accurately describes seasonal and synoptic-scale fluctuations of transported cave gases. As an

immediate application, this theory could be used to improve estimates for production rates of cave gases such as CO<sub>2</sub> and <sup>222</sup>Rn. Currently-used field techniques can be destructive to the cave's fragile environment, but our methodology is completely non-intrusive as it relies only on knowledge of outside temperatures.

A longer-term application is to use these results to improve speleothem interpretation for climate reconstruction. Of course, in this application, neither the internal microclimatic conditions nor the external ones would be known *a priori*. Rather, inferring past climate is inherently an inverse problem, typically treated by representing the climate's influence on the proxy (e.g., speleothem, tree ring, etc.) via a transfer function (i.e., a forward model like ours), and then inverting this transfer function through inverse modeling for climate reconstruction. While it has been recognized that ventilation plays a critical role in speleothem growth, such effects have not yet been quantitatively incorporated into paleoclimate inference models, likely due to the complexity involved. The transparency afforded by our model, however, could prove useful in obtaining tractable transfer functions for climate reconstruction. In particular, we have shown that the ventilation rate can be accurately estimated from knowledge of outside temperature, without requiring internal temperature and climatic variables as additional inputs. Incorporating this theory into existing paleoclimate models, and the subsequent inversion of the transfer function, may allow for better estimates of the corresponding external temperatures (i.e., reconstruct the past climate). In essence, the simpler the forward model, the more feasible inversion becomes.

## Acknowledgments

The authors sincerely thank the management staff of Florida Caverns State Park, especially Kelly Banta, for providing an incredible opportunity to study the DTC. We thank Harley Means at the Florida Geological Survey for invaluable inter-agency facilitation during early efforts to enter and instrument a pristine cave. Thanks to Cameron Ridgewell for creating a 3D map of the DTC and Matt Kalch for his detailed mapping efforts during this study. We thank William Burnett for help with interpreting radon measurements, and William Dewar for inspiring suggestions and comments. The meteorological data from Marianna Airport is obtained from <https://www.ncdc.noaa.gov/cdo-web/>. The input files and results of the numerical calculations are available from the authors upon request ([kk11m@my.fsu.edu](mailto:kk11m@my.fsu.edu)). Finally, we thank two anonymous reviewers and Dr. Sylvia Riechelmann for helping to focus and refine the applications of this study.

## References

- Andrews, J.N., Wood, D.F., 1972, Mechanism of radon release in rock matrices and entry into groundwaters: *Trans Inst Mining Metallurgy*, v. B81, p. 198–209
- Armi, L., 1986, The hydraulics of two flowing layers with different densities: *Journal of Fluid Mechanics*, v. 163, p. 27–58. <https://doi.org/10.1017/S0022112086002197>.
- Baldini, J., McDermott, F., Fairchild, I., 2006, Spatial variability in cave drip water hydrochemistry: Implications for stalagmite paleoclimate records: *Chemical Geology*, v. 235, p. 390–404. <https://doi.org/10.1016/j.chemgeo.2006.08.005>.
- Banner, J.L., Guilfoyle, A., James, E.W., Stern, L.A., Musgrove, M., 2007, Seasonal variations in modern speleothem calcite growth in central Texas, USA: *Journal of Sediment Research*, v. 77, p. 615–622. <https://doi.org/10.2110/jsr.2007.065>.
- Bergman, T.L., Incropera, F.P., 2011, *Fundamentals of heat and mass transfer*: Hoboken, N.J., John Wiley & Sons, Inc., 1050 p.
- Boussinesq, M.J., 1897, *Théorie de l'écoulement tourbillonnant et tumultueux des liquides dans les lits rectilignes a grande section*: Paris, Gauthier-Villars et fils, v. 1.
- Christoforou, C.S., Salmon, L.G., Cass, G.R., 1996, Air exchange within the Buddhist cave temples at Yungang, China: *Atmospheric Environment*, v. 30, p. 3995–4006. [https://doi.org/10.1016/1352-2310\(96\)00123-9](https://doi.org/10.1016/1352-2310(96)00123-9).
- Daëron, M., Drysdale, R.N., Peral, M., Huyghe, D., Blamart, D., Coplen, T.B., Lartaud, F., Zanchetta, G., 2019, Most Earth-surface calcites precipitate out of isotopic equilibrium: *Nature Communications*, v. 10, no. 429. <https://doi.org/10.1038/s41467-019-08336-5>.
- Dalziel, S.B., 1991, Two-layer hydraulics: a functional approach: *Journal of Fluid Mechanics*, v. 223, p. 135–163. <https://doi.org/10.1017/S0022112091001374>.
- Daniel, J., Portmann, R., Solomon, S., Murphy, D., 2012, Identifying weekly cycles in meteorological variables: the importance of an appropriate statistical analysis: *Journal of Geophysical Research* v. 117, no. D13203. <https://doi.org/10.1029/2012JD017574>.
- De Freitas, C., Littlejohn, R., 1987, Cave climate: assessment of heat and moisture exchange: *Journal of Climatology*, v. 7, p. 553–569. <https://doi.org/10.1002/joc.3370070604>.
- Deininger, M., Fohlmeister, J., Scholz, D., Mangini, A., 2012, Isotope disequilibrium effects: the influence of evaporation and ventilation effects on the carbon and oxygen isotope composition of speleothems — A model approach. *Geochimica et Cosmochimica Acta*, v. 96, p. 57–79. <https://doi.org/10.1016/j.gca.2012.08.013>.
- Dreybrodt, W., Hansen, M., Scholz, D., 2016, Processes affecting the stable isotope composition of calcite during precipitation on the surface of stalagmites: Laboratory experiments investigating the isotope exchange between DIC in the solution layer on top of a speleothem and the CO<sub>2</sub> of the cave atmosphere: *Geochimica et Cosmochimica Acta*, v. 174, p. 247–262. <https://doi.org/10.1016/j.gca.2015.11.012>
- Earl, N., Simmonds, I., Tapper, N., 2016, Weekly cycles in peak time temperatures and urban heat island intensity: *Environmental Research Letters*, v. 11, no. 074003. <https://doi.org/10.1088/1748-9326/11/7/074003>.
- Faimon, J., Štelcl, J., Sas, D., 2006, Anthropogenic CO<sub>2</sub>-flux into cave atmosphere and its environmental impact: a case study in the Císařská Cave (Moravian Karst, Czech Republic): *Science of The Total Environment*, v. 369, p. 231–245. <https://doi.org/10.1016/j.scitotenv.2006.04.006>.
- Faimon, J., Troppová, D., Baldík, V., Novotný, R., 2012, Air circulation and its impact on microclimatic variables in the Císařská Cave (Moravian Karst, Czech Republic): *International Journal of Climatology*, v. 32, p. 599–623. <https://doi.org/10.1002/joc.2298>.
- Fairchild, I.J., Baker, A., 2012, *Speleothem science: from process to past environments*: Hoboken, N.J., John Wiley & Sons, Inc., 421 p. <https://doi.org/10.1002/9781444361094>.

- Fairchild, I.J., Borsato, A., Tooth, A.F., Frisia, S., Hawkesworth, C.J., Huang, Y., McDermott, F., Spiro, B., 2000, Controls on trace element (Sr–Mg) compositions of carbonate cave waters: implications for speleothem climatic records: *Chemical Geology*, v. 166, p. 255–269. [https://doi.org/10.1016/S0009-2541\(99\)00216-8](https://doi.org/10.1016/S0009-2541(99)00216-8).
- Fairchild, I.J., Smith, C.L., Baker, A., Fuller, L., Spötl, C., Matthey, D., McDermott, F., 2006, Modification and preservation of environmental signals in speleothems: *Earth-Science Reviews*, v. 75, p. 105–153. <https://doi.org/10.1016/j.earscirev.2005.08.003>.
- Feng, W., Banner, J.L., Guilfoyle, A.L., Musgrove, M., James, E.W., 2012, Oxygen isotopic fractionation between drip water and speleothem calcite: a 10-year monitoring study, central Texas, USA: *Chemical Geology*, v. 304, p. 53–67. <https://doi.org/10.1016/j.chemgeo.2012.02.004>.
- Fernández, P., Gutierrez, I., Quindós, L., Soto, J., Villar, E., 1986, Natural ventilation of the paintings room in the Altamira cave: *Nature*, v. 321, p. 586. <https://doi.org/10.1038/321586a0>.
- Flynn, M., Caulfield, C., 2006, Natural ventilation in interconnected chambers: *Journal of Fluid Mechanics*, v. 564, p. 139–158. <https://doi.org/10.1017/S0022112006001261>.
- Frisia, S., Borsato, A., Fairchild, I.J., McDermott, F., 2000, Calcite fabrics, growth mechanisms, and environments of formation in speleothems from the Italian Alps and southwestern Ireland: *Journal of Sedimentary Research*, v. 70, p. 1183–1196. <https://doi.org/10.1306/022900701183>.
- Frisia, S., Fairchild, I.J., Fohlmeister, J., Miorandi, R., Spötl, C., Borsato, A., 2011, Carbon mass-balance modelling and carbon isotope exchange processes in dynamic caves: *Geochimica et Cosmochimica Acta*, v. 75, p. 380–400. <https://doi.org/10.1016/j.gca.2010.10.021>.
- Gabrovšek, F., Dreybrodt, W., 2000, Role of mixing corrosion in calcite–aggressive H<sub>2</sub>O–CO<sub>2</sub>–CaCO<sub>3</sub> solutions in the early evolution of karst aquifers in limestone: *Water Resources Research*, v. 36, p. 1179–1188. <https://doi.org/10.1029/1999WR900337>.
- Gregorič, A., Vaupotič, J., Šebela, S., 2014, The role of cave ventilation in governing cave air temperature and radon levels (Postojna Cave, Slovenia): *International Journal of Climatology*, v. 34, p. 1488–1500. <https://doi.org/10.1002/joc.3778>.
- Hakl, J., Hunyadi, I., Csige, I., Gécsy, G., Lénárt, L., Várhegyi, A., 1997, Radon transport phenomena studied in karst caves—international experiences on radon levels and exposures: *Radiation Measurements*, v. 28, p. 675–684. [https://doi.org/10.1016/S1350-4487\(97\)00163-7](https://doi.org/10.1016/S1350-4487(97)00163-7).
- Hansen, M., Scholz, D., Froeschmann, M.-L., Schöne, B.R., Spötl, C., 2017, Carbon isotope exchange between gaseous CO<sub>2</sub> and thin solution films: artificial cave experiments and a complete diffusion-reaction model: *Geochimica et Cosmochimica Acta*, v. 211, p. 28–47. <https://doi.org/10.1016/j.gca.2017.05.005>.
- Hansen, M., Scholz, D., Schöne, B.R., Spötl, C., 2019, Simulating speleothem growth in the laboratory: Determination of the stable isotope fractionation ( $\delta^{13}\text{C}$  and  $\delta^{18}\text{O}$ ) between H<sub>2</sub>O, DIC and CaCO<sub>3</sub>: *Chemical Geology*, v. 509, p. 20–44. <https://doi.org/10.1016/j.chemgeo.2018.12.012>.
- Hendy, C.H., 1971, The isotopic geochemistry of speleothems—I: the calculation of the effects of different modes of formation on the isotopic composition of speleothems and their applicability as palaeoclimatic indicators: *Geochimica et Cosmochimica Acta*, v. 35, p. 801–824. [https://doi.org/10.1016/0016-7037\(71\)90127-X](https://doi.org/10.1016/0016-7037(71)90127-X).
- Holman, J., 2002, *Heat transfer*, 9<sup>th</sup> ed.: New York, McGraw-Hill.
- Holton, J.R., Hakim, G.J., 2012, *An introduction to dynamic meteorology*, 5<sup>th</sup> ed.: Boston, Academic Press, 552 p.
- Hunt, G., Linden, P., 1999, The fluid mechanics of natural ventilation—displacement ventilation by buoyancy-driven flows assisted by wind: *Building and Environment*, v. 34, p. 707–720. [https://doi.org/10.1016/S0360-1323\(98\)00053-5](https://doi.org/10.1016/S0360-1323(98)00053-5).
- James, E.W., Banner, J.L., Hardt, B., 2015, A global model for cave ventilation and seasonal bias in speleothem paleoclimate records: *Geochemistry, Geophysics, Geosystems*, v. 16, p. 1044–1051. <https://doi.org/10.1002/2014GC005658>.
- Karmann, I., Cruz Jr, F.W., Viana Jr, O., Burns, S.J., 2007, Climate influence on geochemistry parameters of waters from Santana–Pérolas cave system, Brazil: *Chemical Geology*, v. 244, p. 232–247. <https://doi.org/10.1016/j.chemgeo.2007.06.029>.
- Kowalczyk, A.J., Froelich, P.N., 2010, Cave air ventilation and CO<sub>2</sub> outgassing by radon-222 modeling: how fast do caves breathe?: *Earth and Planetary Science Letters*, v. 289, p. 209–219. <https://doi.org/10.1016/j.epsl.2009.11.010>.
- Lachniet, M.S., 2009, Climatic and environmental controls on speleothem oxygen-isotope values: *Quaternary Science Reviews*, v. 28, p. 412–432. <https://doi.org/10.1016/j.quascirev.2008.10.021>.
- Lambert, W.J., Aharon, P., 2011, Controls on dissolved inorganic carbon and  $\delta^{13}\text{C}$  in cave waters from DeSoto Caverns: implications for speleothem  $\delta^{13}\text{C}$  assessments: *Geochimica et Cosmochimica Acta*, v. 75, p. 753–768. <https://doi.org/10.1016/j.gca.2010.11.006>.
- Matthey, D., Atkinson, T., Barker, J., Fisher, R., Latin, J.-P., Durrell, R., Ainsworth, M., 2016, Carbon dioxide, ground air and carbon cycling in Gibraltar karst: *Geochimica et Cosmochimica Acta*, v. 184, p. 88–113. <https://doi.org/10.1016/j.gca.2016.01.041>.
- McDonald, J., Drysdale, R., Hill, D., Chisari, R., Wong, H., 2007, The hydrochemical response of cave drip waters to sub-annual and inter-annual climate variability, Wombeyan Caves, SE Australia: *Chemical Geology*, v. 244, p. 605–623. <https://doi.org/10.1016/j.chemgeo.2007.07.007>.
- Perrier, F., Richon, P., Sabroux, J.-C., 2005, Modelling the effect of air exchange on <sup>222</sup>Rn and its progeny concentration in a tunnel atmosphere: *Science of The Total Environment*, v. 350, p. 136–150. <https://doi.org/10.1016/j.scitotenv.2004.12.060>.
- Pinchover, Y., Rubinstein, J., 2005, *An introduction to partial differential equations*: New York, Cambridge University Press, 366 p. <https://doi.org/10.1017/CBO9780511801228>.
- Polag, D., Scholz, D., Mühlinghaus, C., Spötl, C., Schröder-Ritzrau, A., Segl, M., Mangini, A., 2010, Stable isotope fractionation in speleothems: Laboratory experiments: *Chemical Geology*, v. 279, p. 31–39. <https://doi.org/10.1016/j.chemgeo.2010.09.016>.
- Pratt, L.J., 2008, Critical conditions and composite Froude numbers for layered flow with transverse variations in velocity: *Journal of Fluid Mechanics*, v. 605, p. 281–291. <https://doi.org/10.1017/S002211200800150X>.
- Richon, P., Perrier, F., Sabroux, J.-C., Trique, M., Ferry, C., Voisin, V., Pili, E., 2005, Spatial and time variations of radon-222 concentration in the atmosphere of a dead-end horizontal tunnel: *Journal of Environmental Radioactivity*, v. 78, p. 179–198. <https://doi.org/10.1016/j.jenvrad.2004.05.001>.
- Sánchez-Moral, S., Soler, V., Cañaveras, J., Sanz-Rubio, E., Van Grieken, R., Gysels, K., 1999, Inorganic deterioration affecting the Altamira Cave, N Spain: quantitative approach to wall-corrosion (solution etching) processes induced by visitors: *Science of The Total Environment*, v. 243, p. 67–84. [https://doi.org/10.1016/S0048-9697\(99\)00348-4](https://doi.org/10.1016/S0048-9697(99)00348-4).
- Scholz, D., Mühlinghaus, C., Mangini, A., 2009, Modelling  $\delta^{13}\text{C}$  and  $\delta^{18}\text{O}$  in the solution layer on stalagmite surfaces: *Geochimica et Cosmochimica Acta*, v. 73, p. 2592–2602. <https://doi.org/10.1016/j.gca.2009.02.015>.
- Sherwin, C.M., Baldini, J.U., 2011, Cave air and hydrological controls on prior calcite precipitation and stalagmite growth rates: implications for palaeoclimate reconstructions using speleothems: *Geochimica et Cosmochimica Acta*, v. 75, p. 3915–3929. <https://doi.org/10.1016/j.gca.2011.04.020>.
- Spötl, C., Fairchild, I.J., Tooth, A.F., 2005, Cave air control on dripwater geochemistry, Obir Caves (Austria): implications for speleothem deposition in dynamically ventilated caves, *Geochimica et Cosmochimica Acta*, v. 69, p. 2451–2468. <https://doi.org/10.1016/j.gca.2004.12.009>.

- Stoll, H., Mendez-Vicente, A., Gonzalez-Lemos, S., Moreno, A., Cacho, I., Cheng, H., Edwards, R.L., 2015, Interpretation of orbital scale variability in mid-latitude speleothem  $\delta^{18}\text{O}$ : significance of growth rate controlled kinetic fractionation effects: *Quaternary Science Reviews*, v. 127, p. 215–228. <https://doi.org/10.1016/j.quascirev.2015.08.025>.
- Tadros, C.V., Treble, P.C., Baker, A., Fairchild, I., Hankin, S., Roach, R., Markowska, M., McDonald, J., 2016, ENSO–cave drip water hydro-chemical relationship: a 7-year dataset from south-eastern Australia: *Hydrology and Earth System Sciences*, v. 20, p. 4625–4640. <https://doi.org/10.5194/hess-20-4625-2016>.
- Tinti, F., Barbaresi, A., Benni, S., Torreggiani, D., Bruno, R., Tassinari, P., 2014, Experimental analysis of shallow underground temperature for the assessment of energy efficiency potential of underground wine cellars, *Energy and Buildings*, v. 80, p. 451–460. <https://doi.org/10.1016/j.enbuild.2014.06.002>.
- Tremaine, D.M., 2010. Speleothem paleoclimatology and modern speleochemistry proxies: Calcite farming in a Continuously Monitored Cave, [http://purl.flvc.org/fsu.fid/FSU\\_migr\\_etd-1523](http://purl.flvc.org/fsu.fid/FSU_migr_etd-1523).
- Tremaine, D.M., Froelich, P.N., Wang, Y., 2011, Speleothem calcite farmed in situ: Modern calibration of  $\delta^{18}\text{O}$  and  $\delta^{13}\text{C}$  paleoclimate proxies in a continuously-monitored natural cave system: *Geochimica et Cosmochimica Acta*, v. 75, p. 4929–4950. <https://doi.org/10.1016/j.gca.2011.06.005>.
- Tremaine, D.M., Froelich, P.N., 2013, Speleothem trace element signatures: a hydrological geochemical study of modern cave dripwaters and farmed calcite: *Geochimica et Cosmochimica Acta*, v. 121, p. 522–545. <https://doi.org/10.1016/j.gca.2013.07.026>.
- Tremaine, D.M., 2015, Dynamic physicochemical influences on speleothem paleoclimate proxy archives: a story of four north Florida caves [Ph.D. Dissertation]: Tallahassee, Florida State University, 267 p. <https://doi.org/10.13140/RG.2.1.2632.0725>.
- Tremaine, D.M., Sinclair, D.J., Stoll, H.M., Lagerström, M., Carvajal, C.P., Sherrell, R.M., 2016, A two-year automated dripwater chemistry study in a remote cave in the tropical south Pacific: using  $[\text{Cl}^-]$  as a conservative tracer for seasalt contribution of major cations: *Geochimica et Cosmochimica Acta*, v. 184, p. 289–310. <https://doi.org/10.1016/j.gca.2016.03.029>.
- Wackerbarth, A., Scholz, D., Fohlmeister, J., Mangini, A., 2010, Modelling the  $\delta^{18}\text{O}$  value of cave dripwater and speleothem calcite: *Earth and Planetary Science Letters*, v. 299, p. 387–397. <https://doi.org/10.1016/j.epsl.2010.09.019>.
- Wang, Y., Cheng, H., Edwards, R.L., Kong, X., Shao, X., Chen, S., Wu, J., Jiang, X., Wang, X., An, Z., 2008, Millennial-and orbital-scale changes in the East Asian monsoon over the past 224,000 years: *Nature*, v. 451, p. 1090. <https://doi.org/10.1038/nature06692>.
- Watkins, J.M., Nielsen, L.C., Ryerson, F.J., DePaolo, D.J., 2013, The influence of kinetics on the oxygen isotope composition of calcium carbonate: *Earth and Planetary Science Letters*, v. 375, p. 349–360. <https://doi.org/10.1016/j.epsl.2013.05.054>.
- Watkins, J.M., Hunt, J.D., Ryerson, F.J., DePaolo, D.J., 2014, The influence of temperature, pH, and growth rate on the  $\delta^{18}\text{O}$  composition of inorganically precipitated calcite: *Earth and Planetary Science Letters*, v. 404, p. 332–343. <https://doi.org/10.1016/j.epsl.2014.07.036>.
- Wigley, T., Brown, C., 1971, Geophysical applications of heat and mass transfer in turbulent pipe flow: *Boundary-layer meteorology*, v. 1, p. 300–320. <https://doi.org/10.1007/BF02186034>.
- Wong, C.I., Banner, J.L., Musgrove, M., 2011. Seasonal dripwater Mg/Ca and Sr/Ca variations driven by cave ventilation: implications for and modeling of speleothem paleoclimate records: *Geochimica et Cosmochimica Acta*, v. 75, p. 3514–3529. <https://doi.org/10.1016/j.gca.2011.03.025>.
- Wong, C.I., Breecker, D.O., 2015, Advancements in the use of speleothems as climate archives: *Quaternary Science Reviews*, v. 127, p. 1–18. <https://doi.org/10.1016/j.quascirev.2015.07.019>.